Semi-analytical, numerical, and CFD formulations of a spherical floater

Spyridon A. Mavrakos, Spyridon K. Zafeiris, Georgios P. Papadakis, Dimitrios N. Konispoliatis

Abstract— **In the present work a semi-analytical model is applied to solve the wave diffraction and the heave radiation-problems around a spherical WEC, in the context of linear potential theory. The applied methodology is based on the discretization of the flow field around the body using coaxial ring elements, which are generated from the approximation of the sphere's meridian line by a stepped curve. For each type of element, the Laplace equation is formulated and an eigenfunction expansion for the velocity potential is made. The latter is approximated with Fourier series which are derived based on the separation of variables principle. The requirements for continuity of the potential function and its derivative at the boundaries of neighboring ring-shaped macroelements are being satisfied.**

The outcomes of the theoretical analysis are supplemented and compared with numerical and high fidelity CFD simulations. Numerical results are given from the comparison of the three formulations, and some interesting phenomena are discussed concerning the accuracy of the applied methodology and the viscous effects on the floater.

Keywords—**CFD formulation, Exciting forces, Hydrodynamic coefficients, Numerical results, Spherical floater, Theoretical methodology**

I. INTRODUCTION

Today, humanity is facing the great pressure of fossil fuels exhaustion and environmental pollution. This obliges governments and industries to make accelerated efforts on producing green energy. The focus is spotted on the marine environment which is a vast source of renewable energy. Among several classes of designs proposed for wave energy conversion, spherical Wave Energy Converters (WECs) have received considerable attention. The problems of water wave diffraction and radiation by a sphere have been examined by a substantial amount of literature, i.e., [1], [2], [3], [4], to name a few, whereas in the works of [5], [6], [7], [8] linear hydrodynamic effects on a spherical WEC have been examined. All these research works are based on potential flow methodologies. Nevertheless, over the last decade there has been a significant interest in Computational Fluid Dynamics (CFD) modelling due to its detailed results, focusing also on spherical WECs [10], [11]. Recently, Kramer et al., [12] conducted highly accurate and precise heave decay tests on a semi-submerged sphere. In their study the experimental outcomes were compared with the results from several numerical models based on linear potential flow, fully nonlinear potential flow, and the Reynolds-averaged Navier-Stokes equations.

In the present work a semi-analytical model is applied to solve the wave diffraction- and the heave radiation-problems around a spherical WEC, which is either semi-submerged or fully submerged under the free surface, in the context of linear potential theory. The outcomes of the theoretical analysis are supplemented and compared with numerical software and high fidelity CFD simulations.

II. MATHEMATICAL FORMULAE

We consider a free-floating submerged sphere of radius a, as depicted in Figure 1. The sphere is considered to be exposed to the action of regular waves with amplitude $H/2$ and wave frequency ω in constant water depth d. The centre of the sphere is located at a distance h below the free surface (see Figure 1). A cylindrical co-ordinate system (r, θ, z) is introduced located at the seabed, with the z-axis pointing upward, whereas a spherical coordinate system (r, θ, φ) is assumed located at the geometric centre of the sphere. In the present semi-analytical formulation, viscous effects are neglected, whereas the fluid is assumed incompressible. Furthermore, the fluid's motions are assumed small, so that the linearized diffraction and radiation problems can be considered. The flow is governed by the velocity potential, $\Phi = Re[\varphi e^{-i\omega}]$, which is written as:

S. A. Mavrakos is Emeritus Professor at School of Naval Architecture and Marine Engineering, National Technical University of Athens, Greece (e-mail: mavrakos@naval.ntua.gr).

S. K. Zafeiris is a PhD Student at School of Naval Architecture and Marine Engineering, National Technical University of Athens, Greece (e-mail: zafeiris_spiros@mail.ntua.gr).

G. P. Papadakis is Assistant Professor at School of Naval Architecture and Marine Engineering, National Technical University of Athens, Greece (e-mail: papis@fluid.mech.ntua.gr).

D. N. Konispoliatis is Assistant Professor at School of Naval Architecture and Marine Engineering, National Technical University of Athens, Greece (e-mail: dkonisp@naval.ntua.gr).

Digital Object Identifier: https://doi.org/10.36688/ewtec-2023-198

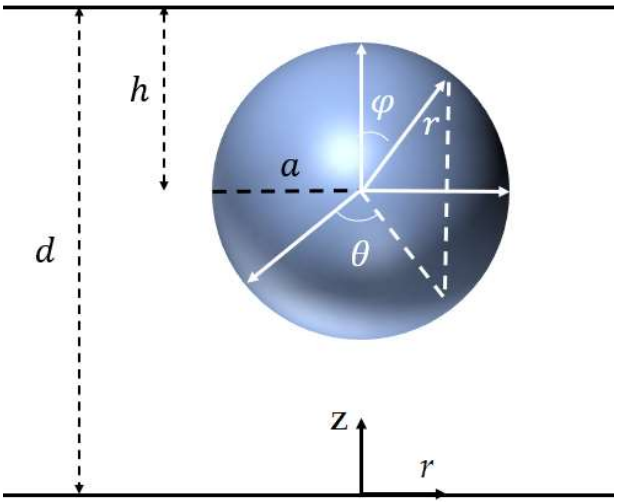

Fig. 1. Schematic representation of the examined spherical absorber.

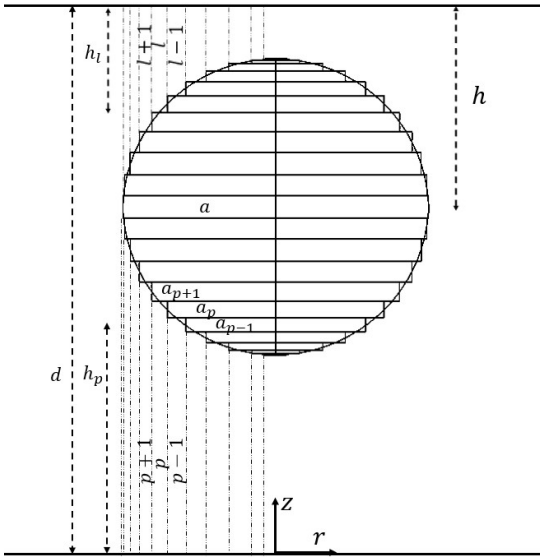

Fig. 2. Discretization of the flow field around a sphere.

$$\varphi = \underbrace{\varphi_0 + \varphi_7}_{\varphi_D} + \dot{\xi}_3 \varphi_3, \tag{1}$$

Here, φ_0 is the velocity potential of the incident harmonic wave, φ_7 is the scattered potential for the sphere fixed in the waves, and φ_3 is the radiation potential induced around the sphere due to its forced heave oscillations with unit amplitude. Also, $\dot{\xi}_3$ denotes the complex velocity potential of the body in heave direction.

The velocity potential of the undisturbed incident wave can be expressed using Jacobis's expansion as:

$$\varphi_0 = -\frac{i\omega H}{2}\frac{\cosh(kz)}{ksinh(kd)}\left[\sum_{m=0}^{\infty} \varepsilon_m\, i^m J_m(kr)\cos(m\theta)\right] \tag{2}$$

Here, J_m denotes the $m-$th order Bessel function of first kind and ε_m is the Neumann's symbol. Also, the wave number and the wave frequency ω are related by the dispersion equation.

In accordance with Equation (2) the diffraction and the heave radiation velocity potentials φ_D, φ_R of the flow field around the sphere are written as:

$$\varphi_D = -\frac{i\omega H}{2}\left[\sum_{m=0}^{\infty} \varepsilon_m\, i^m \Psi_{D,m}(r,z)\cos(m\theta)\right] \tag{3}$$

$$\varphi_3 = \Psi_{3,0}(r,z) \tag{4}$$

The complex velocity potentials φ_D, φ_R have to fulfill the Laplace differential equation in the fluid domain, and the proper boundary conditions on the free water surface and the seabed, and an appropriate condition in far field. Also, the velocity potentials should satisfy the conditions on the sphere's wetted surface S.

For the sphere considered in the present analysis, the diffraction and the radiation wave potentials involved in Equations (3), (4) have been established through the method of matched axisymmetric eigenfunction expansions. According to this method, the flow field around the sphere is subdivided in coaxial ring-shaped fluid regions (see Figure 2), in each of which different series representations of the velocity potentials are made. The adopted series expansions are selected in such a way, that the kinematic boundary condition at the horizontal walls of the sphere, the linearized condition at the free surface, the kinematic one on the seabed and the radiation condition at infinity are a priori satisfied. Using Galerkin's method, the various potential solutions are then matched by the requirements for continuity of the hydrodynamic pressure and radial velocity along the vertical boundaries of adjacent fluid regions, as well as by fulfilling the kinematic conditions at the vertical walls of the sphere. This procedure delivers the linear systems of equations for the determination of the unknown coefficients needed for the series representation of the velocity potential in each fluid region. The method has been extensively presented in [12]. Nevertheless, the expressions for the functions $\Psi_{D,m}, \Psi_{R,0}$ for each macroelement are presented in the Appendix.

Having solved the first order boundary value problem, the exciting forces applied on the spherical floater and its added mass and radiation damping coefficients are calculated as follows:

$$F_\ell = -i\omega\rho \iint_S \varphi_D\, n_\ell dS, \qquad \ell = 1,3,5 \tag{5}$$

$$a_{33} - \frac{i}{\omega} b_{33} = \rho \iint_S \varphi_3\, n_3 dS \tag{6}$$

where S is the sphere's mean wetted surface and n_ℓ are the generalized normal components defined by $n = (n_1, n_2, n_3); r \times n = (n_4, n_5, n_6)$, r being the position vector of a point on the wetted surface with respect to the reference coordinate system of the sphere.

III. CFD Formulation – MaPFlow Solver

The validation is conducted with the use of CFD. The solver in which these numerical experiments were condu-

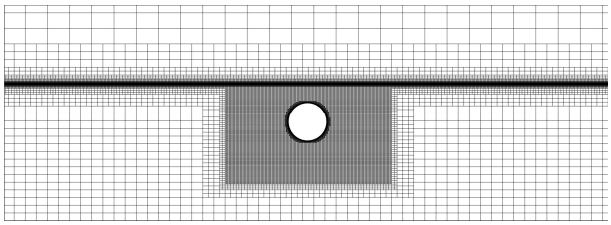

Fig. 3. A slice of the computational domain for the CFD simulations for the fully submerged cylinder. The mesh in the free surface region is refined to capture the incident waves.

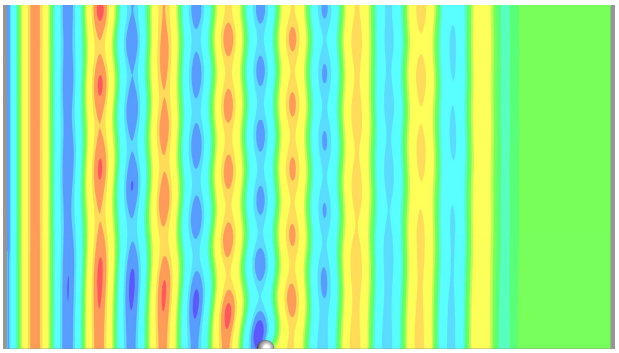

Fig. 4. Wave train propagation for ω=0.90 rad/s

cted is MaPFlow, an in-house developed code that uses the finite volume method to solve the incompressible Navier-Stokes equations and allows for multiphase modelling with the use of the volume of fluid (VOF) formulation. MaPFlow is based on the Artificial Compressibility method (AC) for velocity-pressure coupling and accepts general polyhedral multi-block meshes. In the AC method, an artificial (pseudo-time) derivative is added in the system of equations by introducing the fictitious equation of state $\frac{\partial \rho}{\partial p}|_{\tau} = \frac{1}{\beta}$ allowing to correct the pressure field with the divergence-free constraint in iterative steps. This equation of state assumes a relation between density ρ and pressure p. Also, it contains the artificial speed of sound $\beta > 0$ which is a numerical parameter that controls the convergence. With τ we express the pseudo-time. The iterative procedure is performed implicitly with the use of the Gauss-Seidel method and a linearization of the steady residual (spatial terms). Also, the preconditioner of Kunz [19] is used in order to accelerate the convergence. The augmented system of equations reads:

$$\frac{1}{\beta \rho_m}\frac{\partial p}{\partial \tau} + \nabla \cdot \vec{u} = 0, \tag{7}$$

$$\rho_m \frac{\partial \vec{u}}{\partial \tau} + \vec{u}\frac{\partial \alpha_l}{\partial \tau}\Delta\rho + \rho_m \frac{\partial \vec{u}}{\partial t} + \vec{u}\frac{\partial \alpha_l}{\partial t}\Delta\rho + \nabla \cdot (\rho_m \vec{u} \cdot \vec{u}) + \nabla p = \nabla \cdot \bar{\bar{\sigma}} + F_B \tag{8}$$

$$\frac{\alpha_l}{\rho_m \beta}\frac{\partial p}{\partial \tau} + \frac{\partial \alpha_l}{\partial \tau} + \frac{\partial \alpha_l}{\partial t} + \nabla \cdot (\alpha_l \vec{u}) = 0, \tag{9}$$

Equations (7,8,9) are the continuity, the x-y-z momentum and the advection of the volume fraction. $p, \vec{u}, \alpha_l$ indicate the primitive solution variables. These are the pressure, the velocity vector and the volume fraction respectively. Also, ρ_w is the density of water and ρ_a is the density of air. Lastly, F_B is the vector of all the external forces to the system. We refer to [13] for details on the values of β and the wave generation-absorption inside the computational domain (numerical water tank).

The density of mixture is calculated with the help of the volume fraction $\rho_m = \alpha_l \rho_w + (1 - \alpha_l)\rho_a$. In the same way the dynamic viscosity of mixture is calculated. $\Delta\rho$ is the density difference from heavier to lighter fluid. The tensor $\bar{\bar{\sigma}}$ incorporates the viscous stresses which in our case are equipped with an eddy viscosity turbulence model to account for the energy of subscale interactions. In the case of free surface flows a modified version of the $k - \omega$ *SST* model is used. The reader is referred to [20].

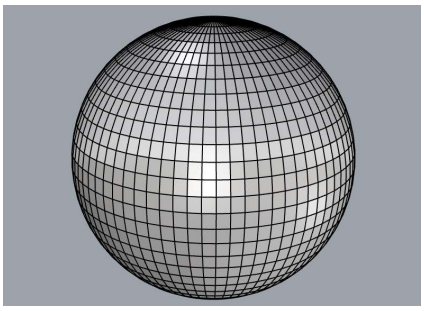

Fig. 5. Discretization of the sphere's wetted surface into 2160 elements for the numerical formulation

In terms of discretization, the solver admits several time-stepping schemes and the recovery of accuracy in space at the interface of computational cells is performed with different reconstruction schemes for every variable ranging from a piecewise linear reconstruction up to compressive reconstruction schemes, which satisfy the hydrostatic variations on pressure. Details can be found in [13], [14]. Finally, the hyperbolic representation of the AC system allows for the use of a Riemann Solver for the convective fluxes. In MaPFlow, the approximate Riemann solver of Roe is used.

In this work, CFD simulations were performed only for the diffraction cases for both the semi and fully submerged sphere. The flow was considered laminar with a first cell height 1e-4 m with 20 layers. The grid was refined in the free surface region to capture the incident waves resulting in CFD mesh composed of 7.5 million cells. The incoming waves are in the linear region with an amplitude of 0.09m. Regarding the mesh resolution it was selected based on the frequency of ω=0.90 rad/s. In the free surface vicinity 20 points per wave height were resolved and 150 points per wavelength. Regarding the time step used, it was chosen based on the wave frequency resulting in 800 steps per wave period. A slice of the computational mesh employed focused near the sphere for the submerged case can be seen in Figure 3. Also, in Figure 4 the wave propagation for the selected ω is depicted.

IV. Numerical Formulation

Based on applied numerical formulation the velocity potential at each point of the field is obtained as the superposition of the potentials due to pulsating

singularities (sources) distributed over the wetted surface of the sphere. Thus, the fluid potential can be written as:

$$\varphi_7(x,y,z) = \frac{1}{4\pi}\iint_S Q(\xi,\eta,\zeta)\, G(x,y,z,\xi,\eta,\zeta) dS \qquad (10)$$

Here $Q(\xi,\eta,\zeta)$ is the strength (i.e. density) of the singularity at (ξ,η,ζ); the $G(x,y,z,\xi,\eta,\zeta)$ is the Green function for finite water depth as given in [15]; x,y,z,ξ,η,ζ are rectangular coordinates and S is the sphere's mean wetted surface.

The Laplace differential and the corresponding boundary conditions are automatically satisfied. By satisfying the kinematic boundary condition on the submerged surface of the sphere, the following integral equations can be obtained:

$$\frac{1}{2}Q_j(x,y,z) + \frac{1}{4\pi}\iint_S Q(\xi,\eta,\zeta)\frac{\partial G(x,y,z,\xi,\eta,\zeta)}{\partial n} dS = -\frac{\partial \varphi_0}{\partial n} \qquad (11)$$

The Eq. (11) is treated by subdividing S in plane quadrilateral or triangular elements with singularities located at the geometrical center of the element. The integral in Eq. (11) is approximated by a finite series of P terms, i.e., P is the number of plane elements. Thus, a linear system of P equations is obtained which is solved with respect to the source's strengths $Q(\xi,\eta,\zeta)$. Once $Q(\xi,\eta,\zeta)$ has been computed for each element the potential of the flow can be easily determined from Eq. (10). The theoretical background of this three-dimensional method is described in detail in [16], [17], [18], thus it is no further elaborated herein. For the present calculations a total of 2160 elements have been applied for the discretization of the sphere's wetted surface (see Fig. 5).

V. SIMULATION & RESULTS

A. Semi-submerged sphere

In the present study a semi-submersible sphere of radius a, floating at a water depth $d = 10a$ is initially considered. Here the center of the sphere is located at the free surface, i.e., $h = 0$. The results from the theoretical formulation are compared with the outcomes from the numerical and CFD analysis. In the latter modelling the computational domain exceeds 40 sphere diameters in the x direction and 30 diameters in the y-direction. Damping zones of length 2 diameters are employed at the domain boundaries. In Table 1 the dimensions of the coaxial ring elements for the hemisphere are depicted. These are applied to the theoretical formulation presented in Section II.

The most consuming part of the theoretical analysis is the evaluation of the Fourier coefficients in each fluid domain. For the present calculations, $i = 70$ and $m = 7$ terms are considered for the velocity representation of the outer fluid domain, whereas $n = 80$ and $m = 7$ for the lower fluid domains.

Table 1: Dimensions of the coaxial ring elements for the semi-submerged sphere

α_1	0.217α	h_1	9.06α
α_2	0.435α	h_2	9.14α
α_3	0.600α	h_3	9.24α
α_4	0.714α	h_4	9.34α
α_5	0.800α	h_5	9.44α
α_6	0.866α	h_6	9.54α
α_7	0.916α	h_7	9.64α
α_8	0.953α	h_8	9.74α
α_9	0.979α	h_9	9.84α
α_{10}	0.995α	h_{10}	9.93α
α_{11}	α	h_{11}	10.00α

In Fig. 6 the horizontal and vertical exciting forces on the semi-submerged sphere are presented. The results are normalized by the factor: $\rho g a^2(H/2)$. It can be seen that the outcomes of the presented methodologies (theoretical and numerical formulations) attain similar results. These are also in excellent agreement with the results from the CFD modelling in terms of the vertical force. Regarding the horizontal force it is evident that CFD simulations predict the peak earlier in the potential formulations. Additionally, the amplitudes of the horizontal force are smaller in the CFD simulations. This is expected since the in the horizontal direction viscous effect are more pronounced.

Fig. 7 depicts the heave hydrodynamic parameters of the sphere, normalized by the term $\rho\alpha^3$ for the hydrodynamic added mass and by $\omega\rho\alpha^3$ for the damping coefficient. The results from the theoretical analysis are compared to the corresponding ones from the numerical formulation with excellent correlation. However, some discrepancies can be observed, regarding the added mass at high values of ω, i.e., $\omega > 0.6$. Hence, the theoretical formulation realized numerically by the coaxial ring-shaped fluid regions should be carefully used.

B. Fully submerged sphere

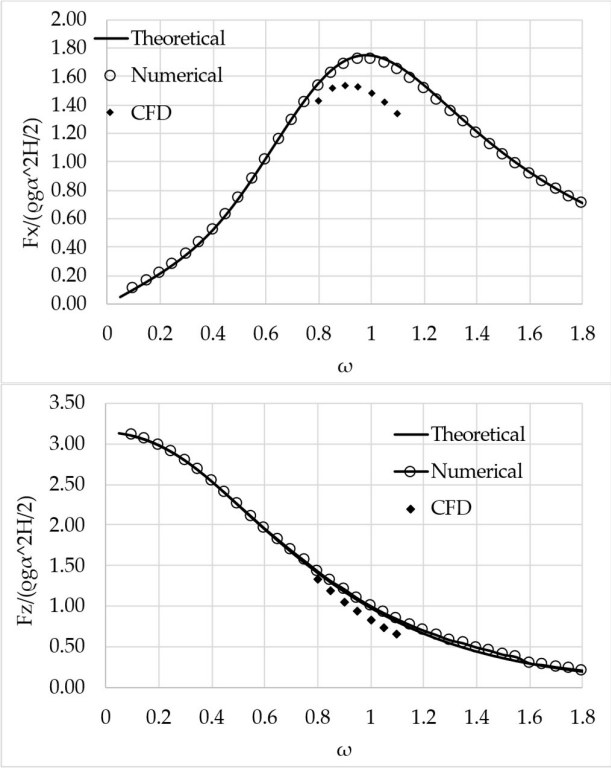

Fig. 6. Non-dimensional exciting forces on the semi-submerged sphere derived by the theoretical analysis: (upper figure) horizontal force; (lower figure) vertical force. The results are compared with the numerical and CFD outcomes.

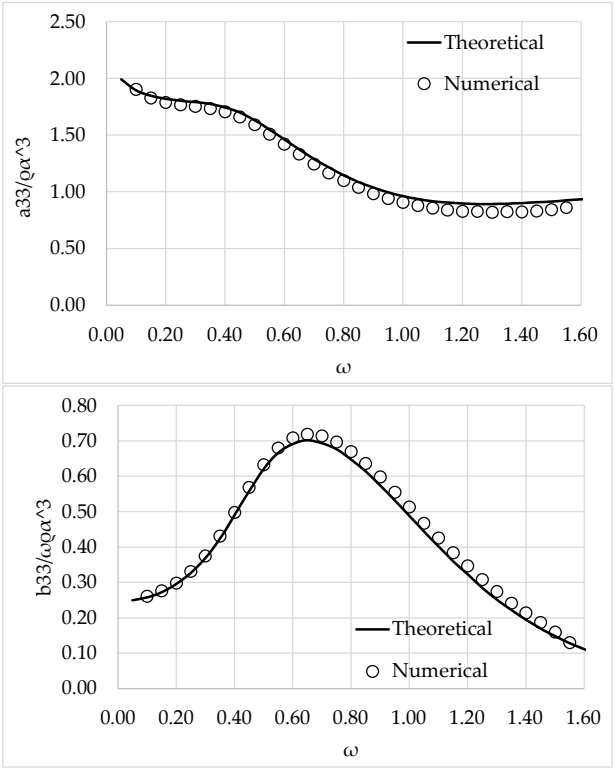

Fig. 7. Non-dimensional hydrodynamic characteristics of the semi submerged spherical floater: (upper figure) heave added mass; (lower figure) heave damping coefficient. The results are compared with the numerical outcomes.

In the sequel the sphere of radius α is considered fully submerged. The distance between the free surface and the body's centre is $h = 2a$, whereas the water depth is remained constant (i.e., $d = 10a$). In Table 2 the dimensions of the coaxial ring elements for the sphere are depicted. The latter are related to the theoretical formulation applied in the present paper. For the present calculations, $i = 70$ and $m = 7$ terms are considered for the velocity representation of the outer fluid domain, $n = 80$ and $m = 7$ for the lower fluid domains, and $i = 70$ and $m = 7$ for the upper fluid domains.

In Fig. 8 the horizontal exciting forces and moments and the vertical exciting forces on the fully submerged sphere are presented. The results are normalized by the factor: $\rho g a^2 (H/2)$ and $\rho g a^3 (H/2)$. Also, in Fig. 9 the heave hydrodynamic parameters of the fully submerged sphere, normalized by the terms $\rho\alpha^3$ and $\omega\rho\alpha^3$ are compared between the two methodologies (theoretical and numerical). It can be seen that the outcomes of the presented methodologies (theoretical and numerical formulations) attain similar results. These are also in excellent agreement with the results from the CFD modelling.

Table 2: Dimensions of the coaxial ring elements for the fully submerged sphere

Radii		h_p		h_l	
α_1	0.217α	h_1	7.00α	h_1	1.00α
α_2	0.435α	h_2	7.06α	h_2	1.06α
α_3	0.600α	h_3	7.15α	h_3	1.15α
α_4	0.714α	h_4	7.25α	h_4	1.25α
α_5	0.800α	h_5	7.35α	h_5	1.35α
α_6	0.866α	h_6	7.45α	h_6	1.45α
α_7	0.916α	h_7	7.55α	h_7	1.54α
α_8	0.953α	h_8	7.65α	h_8	1.64α
α_9	0.979α	h_9	7.74α	h_9	1.75α
α_{10}	0.995α	h_{10}	7.85α	h_{10}	1.84α
α_{11}	α	h_{11}	7.93α	h_{11}	1.93α

As far as the comparisons between the theoretical and the numerical results, regarding the sphere's hydrodynamic coefficients, are concerned, it can be seen that the added mass derived by the theoretical analysis attain in general higher values compared to the ones from the numerical software. Thus, the presented theoretical analysis shows limitations concerning the accurate estimation of the aforementioned physical quantities.

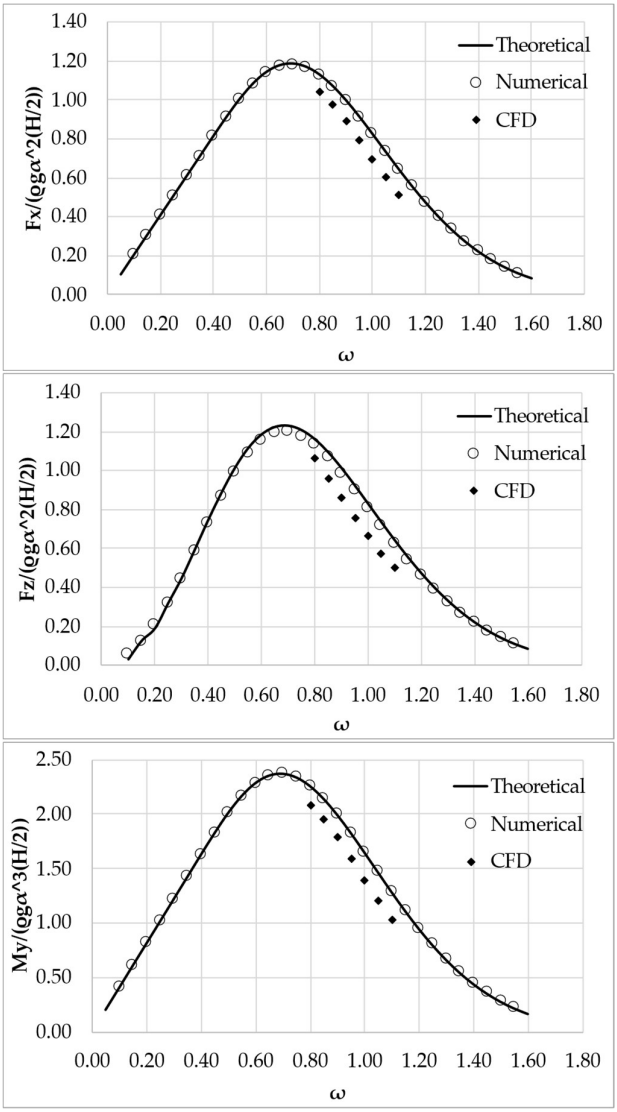

Fig. 8. Non-dimensional exciting forces and moments on the fully submerged sphere derived by the theoretical analysis: (upper figure) horizontal force; (middle figure) vertical force; and (lower figure) horizontal moment. The results are compared with the numerical and CFD outcomes.

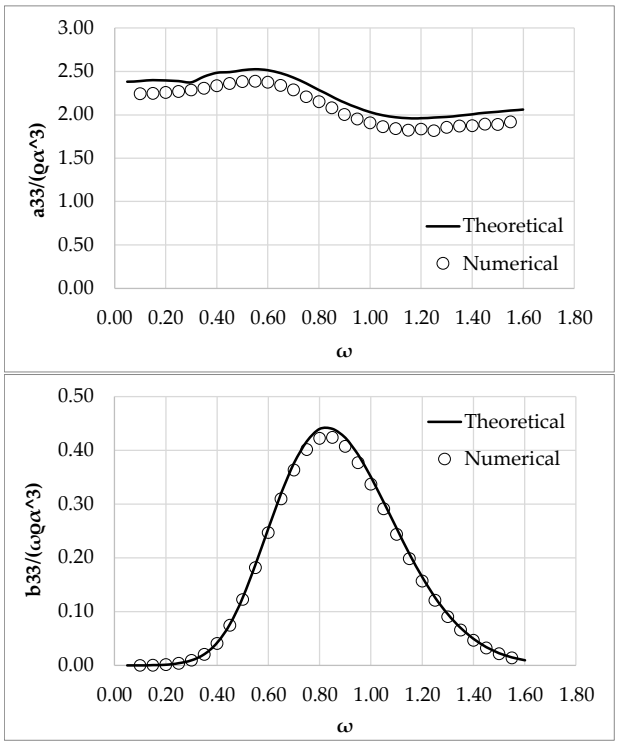

Fig. 9. Non-dimensional hydrodynamic characteristics of the fully submerged spherical floater: (upper figure) heave added mass; (lower figure) heave damping coefficient. The results are compared with the numerical outcomes.

VI. CONCLUSION

In this paper, the exciting forces and the hydrodynamic coefficients of a spherical floater are investigated theoretically in the frequency domain under the action of linear waves. Based on the method of matched axisymmetric eigenfunction expansions, the flow field around the sphere is subdivided in coaxial ring-shaped fluid regions in each of which different series representations of the velocity potentials are made. By comparing the results of the theoretical formulation with numerical and CFD outcomes, the following conclusions were drawn:

- the numerical results and the results from the simulation of the semi-submerged sphere using coaxial ring elements regarding the exciting forces and moments are similar. This holds true also for the fully submerged sphere case;
- the theoretical results for the added mass of the sphere attain some discrepancies compared to their numerical counterparts. These can be traced back to the limitations of the theoretical analysis concerning the accurate estimation of the aforementioned physical quantities of the spherical floater;
- the CFD results are overall in good agreement with the inviscid methodologies. The amplitude of the forces is smaller compared to the potential formulations which is expected due to the viscosity effects. In the case of the semi submerged sphere the peak frequency is predicted earlier than the inviscid methodologies while in the fully submerged case the comparisons are better.

The present investigation can be further extended in order to examine the second order effects on the hydrodynamic performance of a spherical floater under the action of both monochromatic and bichromatic wave trains.

APPENDIX

For each type of the macroelement the following expressions for the functions $\Psi_{D,m}, \Psi_{R,0}$ defined in Equations (3) and (4) are derived:

Outer ring-element ($r \geq a, 0 \leq z \leq d$)

$$\frac{1}{d}\Psi_{j,m}(r,z) = g_j(r,z) + \sum_{i=1}^{\infty} F_{j,m,i}\frac{K_m(a_i r)}{K_m(a_i a)}Z_i(z), \quad j = D,3 \tag{A1}$$

$$g_D(r,z) = \left\{J_m(kr) - \frac{J_m(ka)}{H_m(ka)}H_m(kr)\right\}\frac{Z_0(z)}{dZ'_0(z)}, \quad g_3(r,z) = 0 \tag{A2}$$

The terms H_m, K_m are the m-th order Hankel function of first kind and the modified Bessel function of second kind, respectively. Also, $Z_i$are orthonormal equations equal to:

$$Z_0(z) = \left[\frac{1}{2}\left[1 + \frac{\sinh(2kd)}{2kd}\right]\right]^{-1/2} \cosh(kz) \tag{A3}$$

$$Z_i(z) = \left[\frac{1}{2}\left[1 + \frac{\sin(2a_i d)}{2a_i d}\right]\right]^{-1/2} \cos(a_i z) \tag{A4}$$

where a_i are the roots of the transcendental equation.

Upper ring-elements $(a_p \le r \le a_{p+1}, (d-h_l) \le z \le d, l,p = 1,\dots,10)$

$$\frac{1}{d}\Psi_{j,m}(r,z) = g_j(r,z) + \sum_{i=0}^{\infty}\left[F_{j,m,i}R_{mi}(r) + F^*_{j,m,i}R^*_{mi}(r)\right]Z_i(z), \quad j = D,3 \tag{A5}$$

$$g_D(r,z) = 0, g_3(r,z) = \frac{z}{d} - 1 + \frac{g}{\omega^2} \tag{A6}$$

$$R_{mi}(r) = \frac{I_m(a_i r)K_m(a_i a_p) - I_m(a_i a_p)K_m(a_i r)}{I_m(a_i a_{p+1})K_m(a_i a_p) - I_m(a_i a_p)K_m(a_i a_{p+1})} \tag{A7}$$

$$R^*_{mi}(r) = \frac{I_m(a_i a_{p+1})K_m(a_i r) - K_m(a_i a_{p+1})I_m(a_i r)}{I_m(a_i a_{p+1})K_m(a_i a_p) - I_m(a_i a_p)K_m(a_i a_{p+1})} \tag{A8}$$

The terms I_m is the m-th order modified Bessel function of first kind and $Z_i(z)$ are orthonormal equations which are derived from Equations (A3), (A4) after substituting $d = h_l$ and $z = z - d + h_l$.

Lower ring-elements $(a_p \le r \le a_{p+1}, 0 \le z \le h_p,\ p = 1,\dots,10)$

$$\frac{1}{d}\Psi_{j,m}(r,z) = g_j(r,z) + \sum_{n=0}^{\infty}\varepsilon_n\left[F_{j,m,n}R_{mn}(r) + F^*_{j,m,n}R^*_{mn}(r)\right]cos\left(\frac{n\pi z}{h_p}\right), \quad j = D,3 \tag{A9}$$

$$g_D(r,z) = 0, g_3(r,z) = \frac{z^2 - \left(\frac{1}{2}\right)r^2}{2h_p d} \tag{A10}$$

$$R_{mn}(r) = \frac{I_m\left(\frac{n\pi r}{h_p}\right)K_m\left(\frac{n\pi a_p}{h_p}\right) - I_m\left(\frac{n\pi a_p}{h_p}\right)K_m\left(\frac{n\pi r}{h_p}\right)}{I_m\left(\frac{n\pi a_{p+1}}{h_p}\right)K_m\left(\frac{n\pi a_p}{h_p}\right) - I_m\left(\frac{n\pi a_p}{h_p}\right)K_m\left(\frac{n\pi a_{p+1}}{h_p}\right)} \tag{A11}$$

$$R^*_{mn}(r) = \frac{I_m\left(\frac{n\pi a_{p+1}}{h_p}\right)K_m\left(\frac{n\pi r}{h_p}\right) - I_m\left(\frac{n\pi r}{h_p}\right)K_m\left(\frac{n\pi a_{p+1}}{h_p}\right)}{I_m\left(\frac{n\pi a_{p+1}}{h_p}\right)K_m\left(\frac{n\pi a_p}{h_p}\right) - I_m\left(\frac{n\pi a_p}{h_p}\right)K_m\left(\frac{n\pi a_{p+1}}{h_p}\right)} \tag{A12}$$

whereas for $n = 0$ it holds:

$$R_{m0}(r) = \frac{\left(\frac{r}{a_p}\right)^m - \left(\frac{a_p}{r}\right)^m}{\left(\frac{a_{p+1}}{a_p}\right)^m - \left(\frac{a_p}{a_{p+1}}\right)^m} \tag{A13}$$

$$R^*_{m0}(r) = \frac{\left(\frac{a_{p+1}}{r}\right)^m - \left(\frac{r}{a_{p+1}}\right)^m}{\left(\frac{a_{p+1}}{a_p}\right)^m - \left(\frac{a_p}{a_{p+1}}\right)^m} \tag{A14}$$

For $p = 0$, Equation (A9) can be reformed as:

$$\frac{1}{d}\Psi_{j,m}(r,z) = g_j(r,z) + \sum_{n=0}^{\infty}\varepsilon_n F_{j,m,n}\frac{I_m\left(\frac{n\pi r}{h_0}\right)}{I_m\left(\frac{n\pi a_1}{h_0}\right)}cos\left(\frac{n\pi z}{h_0}\right), \quad j = D,3 \tag{A15}$$

REFERENCES

[1] T. H. Havelock. "Wave due to a floating sphere making periodic heaving oscillations". *Proc. R. Soc. London*, 1955, A231, 1-7.

[2] A. Hulme. "The wave forces acting on a floating hemisphere undergoing force periodic oscillation". *J. Fluid Mech.*, 1982, 121, 443-463.

[3] S. Wang. "*Motions of a spherical submarine in waves". Ocean Engng.*, 1986, 13, 249-271.

[4] G. X. Wu. "The interaction of water waves with a group of submerged spheres". *Appl. Ocean. Res.*, 1995, 17, 165-184.

[5] M. A. Srokosz "The submerged sphere as an absorber of wave power". *J. Fluid Mech.*, 1979, 95(4), 717-741.

[6] G. P. Thomas, D. V. Evans. "Arrays of three-dimensional wave energy absorbers". *J. Fluid Mech.*, 1981, 108, 67-88.

[7] C. M. Linton. "Radiation and diffraction of water waves by a submerged sphere in finite depth". *Ocean Engng.*, 1991, 18, 61-74.

[8] F. Meng, B. Ding, B. Cazzolato, M. Arjomandi. "Modal analysis of a submerged spherical point absorber with asymmetric mass distribution". *Renew. Energy*, 2019, 130, 223-237.

[9] E. A. Shami, Z. Wang, X. Wang "Non-linear dynamic simulations of two-body wave energy converters via identification of viscous drag coefficients of different shapes of the submerged body based on numerical wave tank CFD simulation". *Renew. Energy*, 2021, 179, 983-997.

[10] E. Katsidoniotaki, Z. Shahroozi, C. Eskilsson, J. Palm, J. Engstrom, M. Goteman. "Validation of a CFD model for wave energy system dynamics in extreme waves". *Ocean Engng.*, 2023, 268, 113320.

[11] K. B. Kramer, J. Andersen, S. Thomas, F. B. Bendixen, H. Bingham, R. Read, N. Holk, E. Ransley, S. Brown, Y. Yu, T. T. Tran, J. Davidson, C. Horvath, C. E. Janson, K. Nielsen, C. Eskilsson. "Highly

accurate experimental heave decay tests with a floating sphere: A public benchmark dataset for the model validation of fluid-structure interaction". *Energies*, 2021, 14(2), 269.

[12] K. Kokkinowrachos, S. Mavrakos, S. Asorakos. "Behaviour of vertical bodies of revolution in waves". *Ocean Engng.*, 1986, 13 (6), 505-538.

[13] D. Ntouras, G. Papadakis. "A coupled artificial compressibility method for free surface flows". *J. Marine Sci. Engng*., 2020, 8 (8), 590.

[14] K. Theodorakis, D. Ntouras, G. Papadakis. "Investigation of a submerged fully passive energy-extracting flapping foil operating in sheared inflow". *Journal of Fluids and Structures*, 2022, 113, 103674.

[15] J. V. Wehausen,; E. V. Laitone. "Surface Waves". *Encyclopedia of Physics*, 1960, Vol. 9, Springer Verlag, Berlin, Heidelberg

[16] S. A. Mavrakos,; L. Bardis "Hydrodynamic Characteristics of Large Offshore Units". *The 3rd International Congress on Marine Technology* (IMAM), 1984, Athens, Greece, pp. 505-513.

[17] C. J. Garrison. "Hydrodynamics of large objects in the sea. Part I: Hydrodynamic analysis". *Journal of Hydronautics*, 1974, Vol. 8, No 1.

[18] C. J. Garrison. "Hydrodynamics of large objects in the sea. Part II: Motion of free floating bodies". *Journal of Hydronautics*, 1975, Vol. 9, No 4.

[19] Kunz, Robert F., et al. "A preconditioned Navier–Stokes method for two-phase flows with application to cavitation prediction." *Computers & Fluids* 29.8 (2000): 849-875.

[20] Devolder, Brecht, Pieter Rauwoens, and Peter Troch. "Application of a buoyancy-modified k-ω SST turbulence model to simulate wave run-up around a monopile subjected to regular waves using OpenFOAM®." *Coastal Engineering* 125 (2017): 81-94.